The Journal of Experimental Biology 215, 2359-2368

doi:10.1242/jeb.065615

RESEARCH ARTICLE

Structure and function of the median finfold in larval teleosts

Jos G. M. van den Boogaart, Mees Muller* and Jan W. M. Osse

Wageningen University, Experimental Zoology Group, Wageningen Institute of Animal Sciences (WIAS), Marijkeweg 40, 6709 PG Wageningen, The Netherlands

*Author for correspondence (mees.muller@wur.nl)

SUMMARY

This paper offers a structural and mechanical analysis of the median finfold in larval teleosts. The median finfold is strengthened by bundles of collagen fibres, known as actinotrichia. We demonstrate that these structures contribute to increase the mass of backward accelerated water during swimming. The amount, dimensions, orientation and growth of actinotrichia were measured at various locations along the finfold in several developmental stages of common carp (*Cyprinus carpio*) and zebrafish (*Danio rerio*). Actinotrichia morphology, using light microscopy (e.g. diameter, orientation) and electron microscopy (which revealed their anchoring at proximal and distal ends), correlated with expected lateral forces exerted on the water during swimming. An analytical model is proposed that predicts the extent of camber from the oblique arrangement of the actinotrichia and curvature of the body. Camber of the finfold during swimming was measured from high-speed video recordings and used to evaluate the model predictions. Based on structural requirements for swimming and strain limits for collagen, the model also predicts optimal orientations of actinotrichia. Experimental data confirm the predictions of the model.

Key words: carp, zebrafish, larvae, finfold, actinotrichia, swimming, camber.

Received 13 September 2011; Accepted 15 March 2012

INTRODUCTION

All larval teleosts possess a median finfold (Kendall et al., 1984), which develops prior to hatching inside the egg envelope. In most juvenile and adult fish species, this finfold is gradually resorbed and replaced by separate dorsal, caudal and anal fins. Many species, especially perciform, resorb their median finfold completely before a total body length (TL) of 8 mm is reached [e.g. *Pagrus major* (Fukuhara, 1985)], while others retain a median finfold at TL>35 mm [e.g. *Thymallus thymallus* (Penáz, 1975)].

The larval median finfold consists of a thin double sheet of epidermis extending dorsally, caudally and ventrally from the body in the medial plane, generally covering the caudal two-thirds of the larval body in a pre-flexion larva (flexion refers to the bending of the posterior notochord during the formation of the tail) (Kendall et al., 1984). Post-flexion, the outline of the median finfold gradually becomes less uniform as bony fin rays develop at some locations while the finfold is being resorbed at others. In transverse section, the larval finfold is approximately triangular with a narrow base relative to its height (approximate ratio 1:6) and a rounded top (Fig. 1).

The functional significance of the larval median finfold (Hunter, 1972; Weihs, 1980b; Webb and Weihs, 1986; Wood and Thorogood, 1987; Rombough, 1988; Osse, 1989; Osse, 1990; Liu et al., 1997; Osse and Van den Boogaart, 2004; Rombough, 2004) remains unresolved. The above authors have proposed the following functions: (1) it might be required for effective undulatory swimming at intermediate Reynolds numbers (*Re* 50–1000); (2) the finfold could enhance respiration in pre-hatched larvae by mixing the perivitelline fluid [as assumed in certain diffusion models (Kranenbarg et al., 2000)], and in free-swimming stages by enlarging the body surface; (3) it might reduce sinking speed; (4) it might be necessary for adult fin rays to develop. The diverse proposed functions are not mutually exclusive, and their relative importance might differ among species and change during ontogeny. These proposed functions might help to explain why all fish larvae grow a median finfold despite their often tight energy budget (Wieser, 1995). In this paper we primarily address additional arguments for its role in swimming.

As in tadpoles (Doherty et al., 1998; Wasserzug, 1989), the median finfold of fish larvae lacks bony or cartilage support. In the tail fin of tadpoles (Doherty et al., 1998), collagen fibres oriented at ~45 deg help the tail fin to stay upright during swimming (see also Liu et al., 1997). In larval fish, the finfold is strengthened by left and right arrays of actinotrichia (Ryder, 1886). Actinotrichia are ubiquitous in larval teleosts and have a function in the development (Wood and Thorogood, 1987) and regeneration (Santos-Ruiz et al., 2001) of teleost fins. Actinotrichia are made of elastoidin (Bouvet, 1974; Zhang et al., 2010), ‘the components of which, apart from collagen, are unknown’ (Zhang et al., 2010). Elastoidin is thought to have mechanical properties intermediate between those of collagen and elastin. The ultrastructure of actinotrichia shows a cross-striation of about 65 nm, similar to collagen (Géraudie and Landis, 1982). During ontogeny, individual actinotrichia increase both in length and in width as a result of apposition of fibrils (Géraudie, 1984). During the period of transformation from larva to juvenile, actinotrichia can be replaced by bony lepidotrichia and eventually disappear except at the fin edge of adult teleosts (Géraudie, 1984).

The architecture of the median finfold of fish larvae must be able to cope with the lateral forces during swimming. The median finfold is subjected to high-frequency (>50 Hz), high-amplitude movements during swimming, which results in high reactive forces exerted by

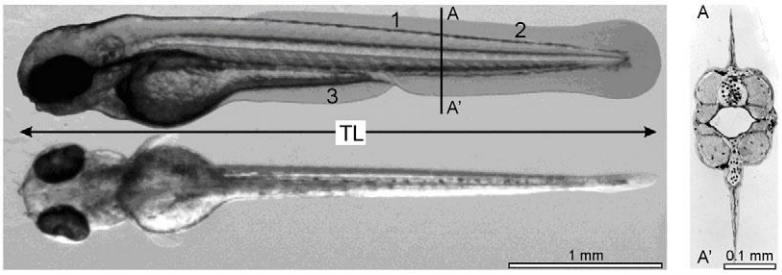

Fig. 1. Lateral (top), dorsal (bottom) and cross-sectional (A–A′, right) view of a zebrafish (*Danio rerio*) larva at 4 days post-fertilization (d.p.f.). TL, total body length; 1, 2 and 3 indicate the dorsal, caudal and pre-anal sites, as explained further in Materials and methods.

the water, suggesting that the finfold needs mechanical support elements (Doherty et al., 1998). In the present paper, we examined whether the actinotrichia can serve this function (see also Dane and Tucker, 1985). We chose carp and zebrafish as model species because we have access to an extensive data bank on their larval swimming kinematics. Osse and colleagues (Osse, 1990; Osse and Van den Boogaart, 2000) showed that carp (*Cyprinus carpio*) larvae change swimming style from anguilliform to (sub)carangiform when reaching the flexion stage at about 7.5 mm TL. In anguilliform swimming, the main thrust is provided by a large amplitude propulsive wave over both trunk and tail (Weihs, 1980a; Batty, 1984) while in (sub)carangiform swimming, the tail and the tail fin create the main thrust (Osse, 1990; Osse and Van den Boogaart, 2000). Zebrafish larvae tend to decrease the lateral amplitude along the undulating trunk (except for the first tail beat) as they change from cyclic to burst-and-coast swimming at the onset of feeding (Müller and Van Leeuwen, 2004).

Our hypotheses were: (i) the functional relevance of the architecture of the median finfold and its changes during ontogeny can be derived from locomotory demands (Weihs, 1980a; Verhagen, 2004), and (ii) the extent of the deformation of the median finfold is controlled passively during swimming.

With respect to (i) we expected a rather uniform structural rigidity of the median finfold in the youngest pre-flexion larvae, whereas in the older pre-flexion larvae, the stiffness of the finfold should increase in the tail region as they change swimming style (Osse and Van den Boogaart, 2000). With respect to (ii) we expected passive camber [lateral tilting of the finfold to the convex side during bending of the body (Van der Stelt, 1968)], caused by the morphology of the median finfold.

To test our predictions, we examined density, dimensions, orientation and anchoring of actinotrichia at several locations in the finfold of carp and zebrafish throughout the larval period. Deformation of the median finfold was studied in free swimming and artificial bending of the larval body. We used a simple analytical model to identify the main factors determining the mechanical behaviour of the finfold during bending of the larval body.

MATERIALS AND METHODS

Animals

Adult carp (*C. carpio* L.) from our laboratory stock were artificially spawned and eggs were fertilized and kept in 22.5 l aquaria in well-aerated water at 24°C. Larvae were fed *Artemia* nauplii, which were supplied *ad libitum* twice a day. Dry food pellets were added to the diet 5 days post-hatching. Adult zebrafish [*Danio rerio* (F. Hamilton 1822)] from our laboratory stock were triggered to spawn, and larvae were raised in 5 l beakers at 28.5°C as described previously (Westerfield, 1993). They were fed unicellular organisms, mainly *Paramecium*, during the first week. The diet was gradually changed to *Artemia* nauplii and TetraMin flake food. Before being handled, larvae were anaesthetized using 100 mg l^{-1} tricaine methanesulphonate (TMS, Sandoz, Basel, Switzerland).

Morphological observations

The width and height of the larval trunk and median finfold were measured on 5 μm cryostat sections. To this end, larvae were anaesthetized in TMS, oriented in 1.5% low gelling agarose dissolved in PBS, frozen in liquid nitrogen and mounted on a stub using Tissue-tec. Individual actinotrichia were measured *in vivo*. Larvae from different length classes were put in a small glass chamber filled with Holfreter solution to enable photographs to be taken of one of the two arrays of actinotrichia (Nikon microphot-FXA microscope equipped with Nomarski differential interference optics at a magnification of ×400) (Westerfield, 1993). We determined numbers of actinotrichia per unit length, and their diameters and angles (α, see Fig. 2) at various sites (Fig. 1) along the intact finfold for five different age groups in carp [2 (hatching), 5, 7, 9 and 11 days post-fertilization, d.p.f.] and three age groups in zebrafish (7, 14 and 21 d.p.f.). Data are presented with respect to TL rather than age, as developmental stages can vary greatly with age but less so with size (Fuiman et al., 1998). Actinotrichia were measured at the following sites (see Fig. 1): (1) the dorsal finfold directly dorsal of the anus, later referred to as the dorsal site; (2) the dorsal finfold, halfway between site 1 and the notochord tip (caudal site); and (3) the middle of the (ventral) pre-anal finfold (pre-anal site). Because of the time-consuming nature of this measurement protocol, we gathered complete data sets for two larvae of each species in each age group. Data from the older larvae appeared to be consistent with data from the younger larvae, so to check whether our measurements were representative for each site and age, five additional larvae of both species at each age were inspected qualitatively. As tensile strength is proportional to cross-sectional area (CSA) (Nash, 1977), we calculated the mean CSA from the diameters of all the individual actinotrichia measured for a given site and age, assuming a circular cross-section (Wood and Thorogood, 1987). This assumption is supported by the elliptic appearance of the cross-section of the actinotrichium in Fig. 6D,E where the long radius of the ellipsis is about double the short radius and the actinotrichium is cut at an angle of ~60 deg (angle α in Table 1).

To determine how actinotrichia are anchored at their proximal and distal ends, samples were prepared for light microscopy and transmission electron microscopy using standard fixation and staining procedures. Transmission electron microscopy pictures were taken using a Philips EM-208.

Experimental observations

To test whether the median finfold is cambered passively or actively, pre-flexion larvae of carp and zebrafish were anaesthetized and their bodies bent manually into a C-shape, closely corresponding

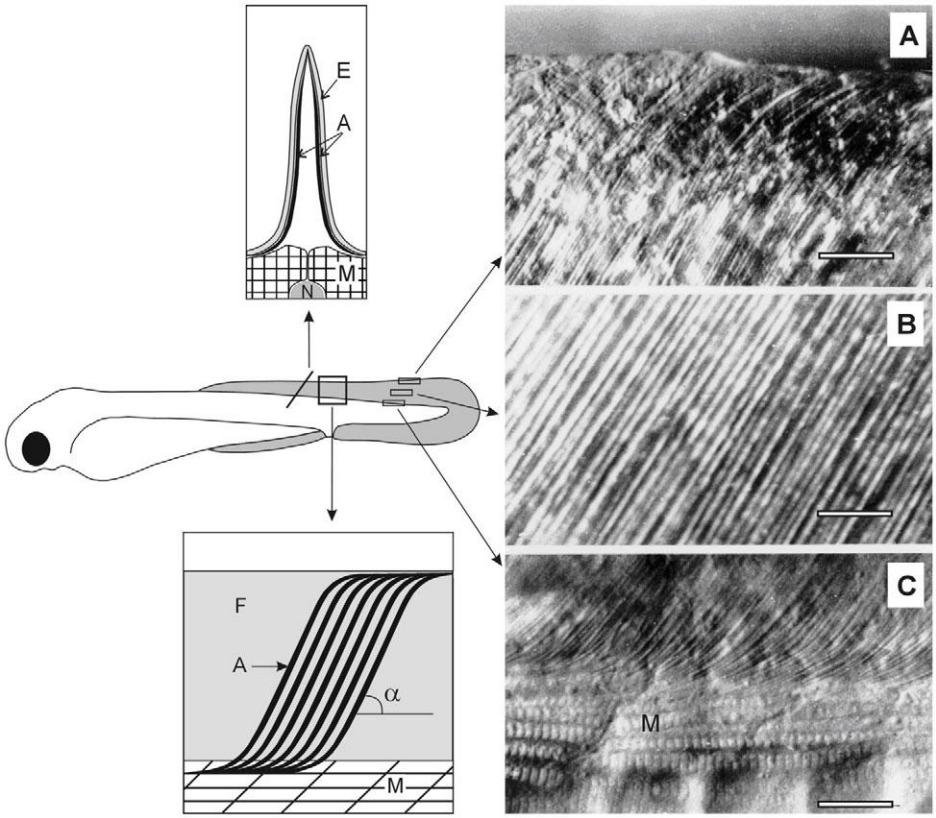

Fig. 2. Left: schematic overview of architecture of the median finfold and orientation of the actinotrichia (top, cross-sectional view; middle and bottom, lateral view). Right: photographs taken with Nomarski differential interference contrast (DIC) of actinotrichia in the finfold (site 2) at (A) the outer edge of the finfold (the thin upper ends bend caudad), (B) halfway up the height of the finfold, running parallel to each other and at an angle with respect to the body axis, and (C) at the proximal end of the actinotrichia (the tapering ends bending rostrad). Scale bars represent 5 μm. α, angle between the actinotrichia and the longitudinal body axis; A, actinotrichia; E, epithelium; F, median finfold; M, myotomes; N, notochord.

to body shapes adopted during fast start escape movements, and the induced deformations of the median finfold were photographed. To obtain qualitative and quantitative observations of camber of the median finfold during swimming movements, we used a high-speed video system (Weinberger SpeedCam 512, Hanshofer Electronic, Nürnberg, Germany) at 1000 frames s^{-1}. Larvae were stimulated to swim through a mirror construction similar to that described elsewhere (De Groot and Van Leeuwen, 2002) in a 6×2.5×2.5 cm aquarium (Fig. 3). This resulted in video images giving a posterior view of a swimming larva, together with three simultaneous projections of the larval body: one mid-dorsal projection and two projections at 45 deg to the medial plane (at 90 deg with respect to each other). Quantitative data of the radius of curvature of the larval body (represented by r_1) and camber of the dorsal and ventral finfold (represented by angle β, Fig. 4) were derived from individual video frames (Fig. 3, right) using AnalySIS software (Olympus Europe, Hamburg, Germany). Radius of curvature (r_1) was determined by manually fitting a circle over the curved part of the body axis adjacent to the site of interest on the mid-dorsal projection if, on the same frame, the lateral projection or posterior view showed camber. Camber angle β was determined from the angle between two lines fitted along the dorsal and ventral part of the cambered finfold, respectively (Fig. 5E). To avoid personal bias, all visual fitting procedures were repeated by two experienced colleagues to test repeatability. Only images with sufficient contrast and optimal projections of the larval body were used (e.g. exact mid-dorsal projection, negligible roll along the length axis of the body). The accuracy of angle β measurements was estimated to be about 3 deg.

Table 1. Mean (±s.d.) angle α (deg) of actinotrichia with respect to the longitudinal body axis at the dorsal (1), caudal (2) and pre-anal (3) site of carp (*Cyprinus carpio*, *N*=8) and zebrafish (*Danio rerio*, *N*=12)

Site	Carp	Zebrafish
1	54.9±1.9	65.6±9.5
2	59.6±2.6	62.6±5.3
3	53.8±10.8	67.2±6.9

Calculations (see Fig. 5)

Model assumptions

We proposed a model to investigate whether the observed arrangement of actinotrichia guides deformation of the larval finfold. The model is based on the following observations and assumptions: (1) in cross-section, the finfold has a triangular shape; (2) the left and right pair of actinotrichia at the flanks of the finfold act as obliquely placed stiff rods during bending of the body; (3) the finfold is filled with incompressible fluid; and (4) longitudinal compression of the notochord centre is ignored. As the body bends, the flank at the convex side forms a wider curve, stretching the outer row of actinotrichia and pulling the top of the finfold out of its original medial position. It is likely that the incompressible fluid is displaced with respect to the fibrous components when the body curves. However, this could not be observed, nor did we find any morphological structures or compartments regulating such a displacement.

To simplify the model, we approximated the trunk of the fish larva as a beam with an elliptical cross-section. Attached to the dorsal and ventral side of this beam are thin vertical sheets of flexible material – the finfold – which form narrow triangles in cross-section (Fig. 5A). The combined mechanical effect of the incompressibility of the tissue and the tensile stiffness of the actinotrichia is captured in the model by the oblique stiff rods, attached parallel to the beam

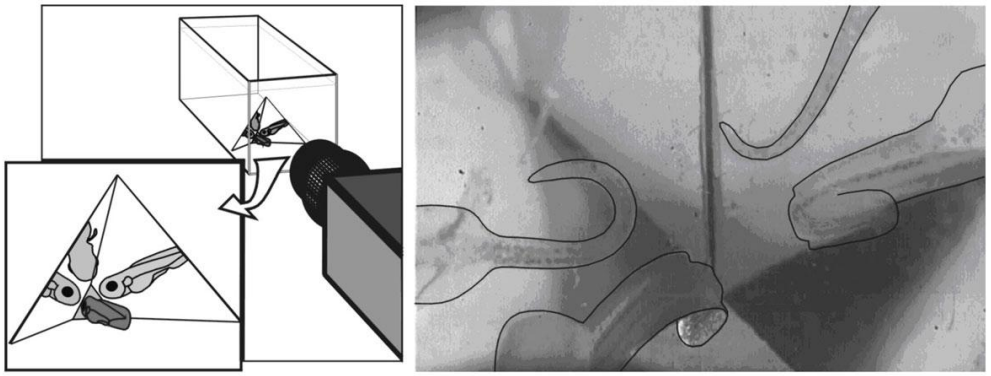

Fig. 3. Left: schematic representation of the filming set-up. Inset: the fish larva (dark grey) is stimulated to swim through a hole at the end of the mirror construction. One mid-dorsal and two 45 deg dorso-lateral projections (light grey) can be seen simultaneously in the mirrors. Right: part of a video frame of a 5 mm TL carp larva, swimming through the mirror construction. Outlines of the larva are shown for clarity.

in a dorso-ventral view and at a fixed angle α with the longitudinal axis (from a lateral view, Fig. 5B). These rods are embedded in the beam (or body) at the proximal ends and remain at a 90 deg angle with the radius of curvature (Fig. 5C) when the body curves. When the beam is bent, the stiff rods, which run at acute angles α with the beam, cause the vertical sheets to form a curved surface in a dorso-ventral view that deviates from the curved median plane of the beam [called camber (Van der Stelt, 1968)]. Rods that are perpendicular to the longitudinal axis would not induce camber. This camber increases as the beam is increasingly bent. The camber increases the beam's second moment of area, i.e. the beam's resistance to bending in the direction of the bending radius r (Nash, 1977). The model quantitatively predicts camber and its effect on the second moment of area as a function of the insertion angle of the actinotrichia, their length and the radius of curvature of the body. It thereby provides a quantitative hypothesis about optimal structural rigidity and maximal force-transmitting surface area.

Model calculations

Bending a beam with a radius of curvature r_1, causes the edge of the finfold to bend with a radius r_2, with r_2 being larger than r_1 (Fig. 5C,D). The difference between r_2 and r_1 depends on the dorsal projection length of the actinotrichia, $l\cos\alpha$, assuming a constant r_1 along the portion of the trunk of the fish under consideration:

$$r_2 = \sqrt{r_1^2 + l^2\cos^2\alpha}\,. \quad (1)$$

The deviation, d (Fig. 5C–E) of the finfold edge from the fish axis is represented by:

$$d = r_2 - r_1\,. \quad (2)$$

Angle β [the angle of deviation of the finfold from the vertical (medial) plane, Fig. 5C,E] can be calculated according to:

$$\beta = 2\arctan\left(\frac{l\sin\alpha}{d}\right). \quad (3)$$

For actinotrichia of a given length l and a segment of the finfold of given length L, the lateral projection area of the finfold A_{lat}, i.e. the force-transmitting surface, is determined by α:

$$A_{lat} = L\,(h_{trunk} + 2l\sin\alpha)\,, \quad (4)$$

where $l\sin\alpha$ is the lateral projection height of the finfold. A lower value of α implies that more camber (larger β) will occur. At the same time the lateral projection area (A_{lat}) decreases, which leads to less area available to generate propulsive forces. Camber also depends on the beam's radius of curvature (r_1). A higher curvature of the larval body (smaller r_1) induces higher camber (larger β).

By bending its body, the fish lengthens the outer edge of the finfold. The corresponding strain ε is:

$$\varepsilon = \frac{r_2 - r_1}{r_1} = \frac{d}{r_1}\,. \quad (5)$$

RESULTS

Morphology

We investigated morphological features to explain the architecture of the median finfold, its change during ontogeny as a result of locomotory demands and its deformation during swimming.

In cross-section, the median finfold of pre-flexion larvae has a triangular shape. The ratio of height to width at the base behind the yolk sac is 4.5 and 4.6 in carp and zebrafish larvae, respectively, and increases gradually to 6.5 and 6.8, respectively, near the caudal tip of the notochord. In both species, the height to width ratio of the body is about 2.2 in the caudal two-thirds of the body.

In lateral view, actinotrichia appear as elongated rods that are curved at both ends (Fig. 2), and situated just under the epithelium on both lateral sides of the median finfold. The diameter of an actinotrichium is nearly constant for most of its length (Fig. 2B), where it runs straight, under an acute angle with respect to the longitudinal body axis. At its base, the tapering end of the actinotrichium bends rostrad (Fig. 2C), and at the outer edge of the finfold it bends caudad (Fig. 2A).

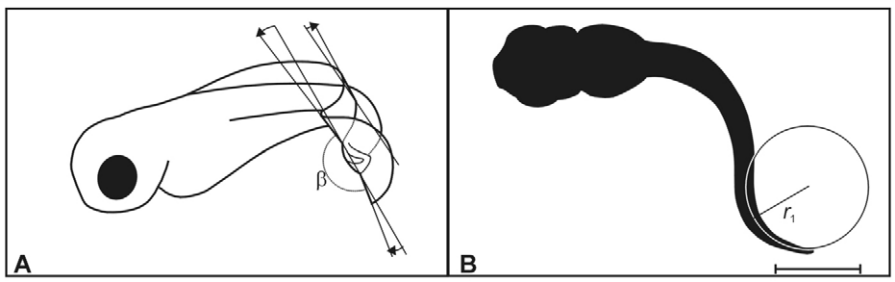

Fig. 4. (A) Drawing of a swimming 5 mm TL carp larva, recorded with high-speed video (500 frames s^{-1}). (B) Silhouette of the mid-dorsal projection of the same larva. Because of the S-curve of the body, two opposite directions of camber can be observed. From these video frames, the radius of curvature r_1 and camber angle β were measured using AnalySIS software. Scale bar indicates 1 mm.

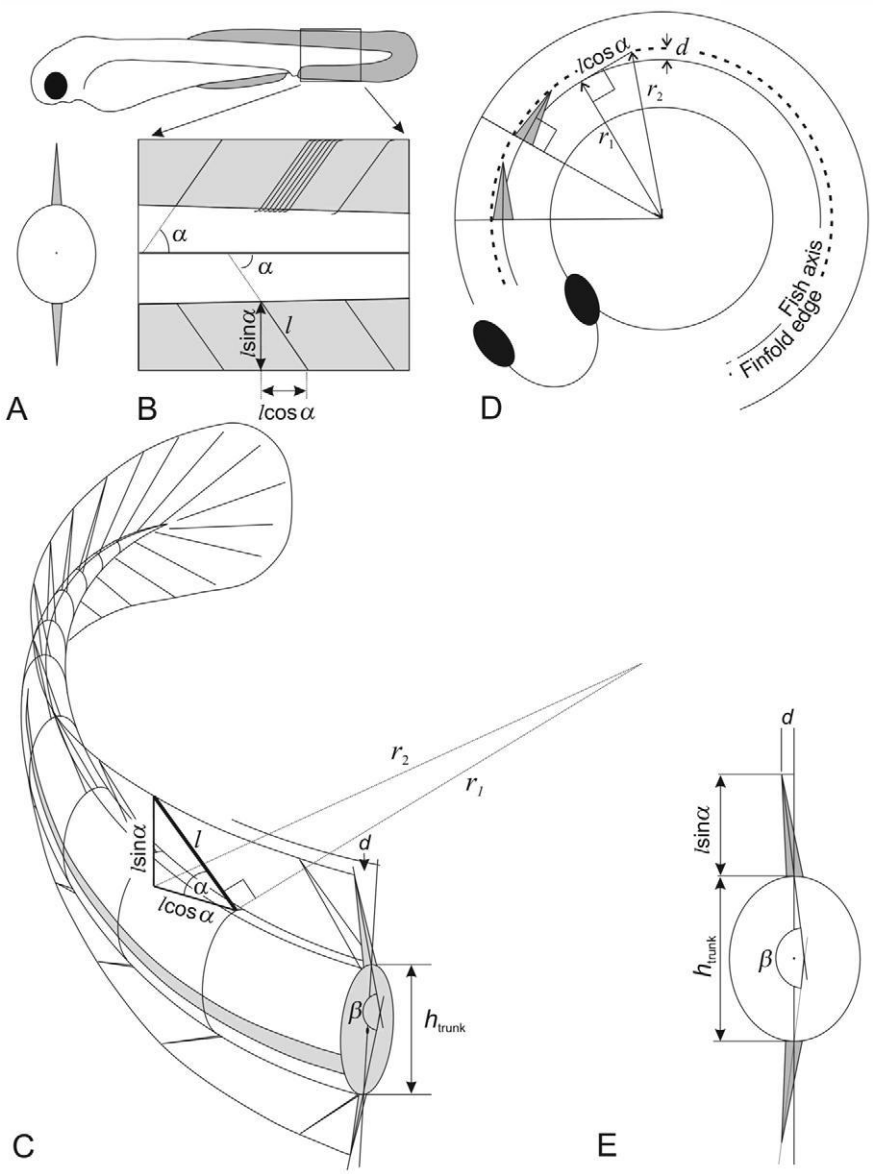

Fig. 5. Model of camber of the finfold. (A) Cross-sectional view. (B) Lateral view. (C) Dorso-caudal view, in perspective. (D) Dorsal view, schematic diagram. (E) Cross-sectional view with camber, schematic diagram. β, angle of camber; *d*, deviation of finfold edge with respect to the fish axis; h_{trunk}, height of the trunk; *l*, length of the actinotrichia; *l*cosα, dorso-ventral projection of *l*; *l*sinα, lateral projection height of the finfold; r_1, radius of curvature of fish axis; r_2, radius of curvature of finfold edge.

Actinotrichia radiate as straight rods from notochord to finfold edge only in the tail tip. All actinotrichia run parallel to their neighbours along most of their length. The overall mean angle α is 56 deg in carp larvae and 64 deg in zebrafish larvae. At sites 1 and 2 (Fig. 1), inter-individual variation of angles is low in carp larvae. Zebrafish larvae show slightly more variation at these sites and in general have higher values. Angles in the pre-anal finfold of both species show more variation. In both species, site 2 shows angles close to 60 deg (Table 1).

Electron microscopy observations (Fig. 6) revealed cross-striation that is specific for collagen. Furthermore, *in situ* hybridization shows collagen type 2*a*1 mRNA expression just under the epithelium in the finfold of 3 d.p.f. zebrafish larvae (Yan et al., 1995). As all observed structural features correspond to collagen, from now on we will treat it as collagen, although some authors have called it elastoidin (Bouvet, 1974), or have even found two additional protein components (Zhang, 2010). Electron microscopy further revealed that at the proximal end, bundles of collagen forming the actinotrichia comprise separate interwoven collagen fibres, forming a layer just below the basal lamina on both sides of the trunk (Fig. 6C,F). These well-organized dermal layers of collagen are part of the dermal skeleton of fish (Sire et al., 1997). At the site of the median finfold, however, the width of this layer of collagen fibres arranged crosswise decreases while the diameter of the actinotrichia increases from their proximal end towards the straight middle part (Fig. 6C,D). No such collagen layer was found along the remaining part of the actinotrichia (Fig. 6D,E). Relatively few individual collagen fibres can be seen at the outer edge of the finfold (Fig. 6B). Here, they are not arranged in a plait, as observed at the base, but individual fibres mingle between the tapering tips of the actinotrichia. At the outer edge, transversely running thin bundles of collagen interconnect left and right pairs of actinotrichia (Fig. 6B). Fibrocytes, which lie under the basal lamina, show a high level of activity, as indicated by the high amount of rough endoplasmatic reticulum (Fig. 6E).

Dimensions and growth of actinotrichia during ontogeny

Although the diameter of an individual actinotrichium varies little along its length, this diameter does change as the larva grows. In carp larvae, diameters range from a minimal value of 0.27 μm

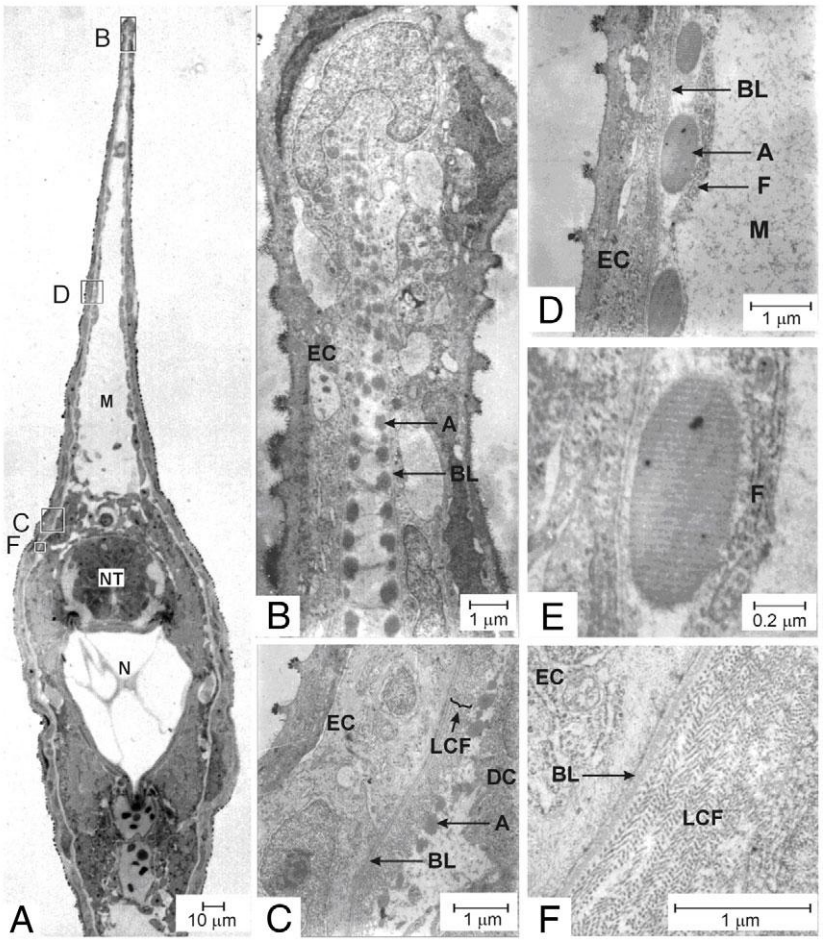

Fig. 6. (A) Light microscopy overview of a cross-section of the dorsal finfold and the trunk of a 6 mm TL carp larva. (B–D) Electron microscopy photographs of the top, base and middle of the finfold. (E) Magnification of D, showing a cross-striation typical for collagen. (F) Magnification of the layer of collagen fibres arranged cross-wise, just below the basal lamina, at the proximal end of the actinotrichia. A, actinotrichium; BL, basal lamina; DC, dermal cells; EC, ectodermal cells; F, fibrocyte; LCF, layer of collagen fibres; N, notochord; NT, neural tube; M, mesenchyme.

(CSA=0.057 μm ^{2}) in larvae of 4.8 mm TL at the dorsal site to a maximal observed value of 2.54 μm (CSA=5.067 μm^2) in 11 mm TL larvae at the caudal site. The mean CSA (calculated for each site and age), assuming a circular cross-section (Wood and Thorogood, 1987), ranges from 0.233 μm^2 at the dorsal site in 4.8 mm TL carp larvae to 3.057 μm^2 at the pre-anal finfold in 11 mm TL carp larvae (Fig. 7A), a more than tenfold increase. Zebrafish larvae have more slender and less variable fibres: diameters range from a minimal measured value of 0.42 μm (CSA=0.139 μm^2) at the dorsal site of 4.1 mm TL larvae to 0.78 μm (CSA=0.478 μm^2) at the caudal site in 6.7 mm TL larvae; the mean CSA ranges from 0.217 to 0.442 μm^2 at the corresponding sites (Fig. 7B).

CSA of actinotrichia at the dorsal sampling site (site 1) in carp slightly increases until flexion (about 7 mm TL). In post-flexion carp larvae, CSA slightly decreases at this site (Fig. 7A). At the caudal sampling site (site 2), CSAs not only have higher values at hatching but also area increases to a much higher value than at site 1, again decreasing slightly in post-flexion larvae. At both sites, actinotrichia are absent in carp larvae of >10 mm TL; by then the larval median finfold has been almost completely resorbed, and the tail blade has been completely invaded by osseous fin rays. In the pre-anal finfold of carp larvae (site 3), actinotrichia could not be found in the smallest size class. One additional 6 mm TL specimen was measured to get some extra data from a pre-flexion stage. The values indicate a small mean CSA until a TL of 10 mm. At TL>10 mm, a rapid increase in CSA can be seen, suggesting a different role for this part of the larval median finfold in carp.

In zebrafish, CSA gradually increases at all three sites (Fig. 7B). The data do not show the same trend at the length class at which flexion occurs, unlike in carp larvae. Above 7 mm TL, zebrafish have resorbed their larval median finfold at sites 1 and 2 and here, in addition, actinotrichia in the tail blade have been replaced by osseous fin rays (lepidotrichia).

Experiments

Experiments were done to investigate how the finfold deforms during swimming. In the experiment in which anaesthetized larvae (N=5 in both species) were bent manually (underwater), the finfold cambered from its original medial plane in the expected convex direction, opposite to the bending direction of the body (Fig. 8). This means that camber is passive, imposed by the structure of the finfold and induced by bending of the body. Additionally, when 1 day old carp larvae (TL=5.2 mm, N=3) were bent in the same way, camber was not observed in the pre-anal finfold, while it was observed in the caudal finfold (Fig. 9). This observation agrees with the absence of actinotrichia in the pre-anal finfold of carp larvae of <6 mm TL, in contrast with the caudal finfold where actinitrichia are present in this size class.

From high-speed video recordings, about 200 swimming movements of pre-flexion larvae were selected for further analysis. In all these recordings, we observed camber in the finfold, but in most recordings either one of the projections was out of focus or there was insufficient contrast to allow reliable measurements. In 34 scenes, of which 19 were from carp larvae, frames could be selected with an

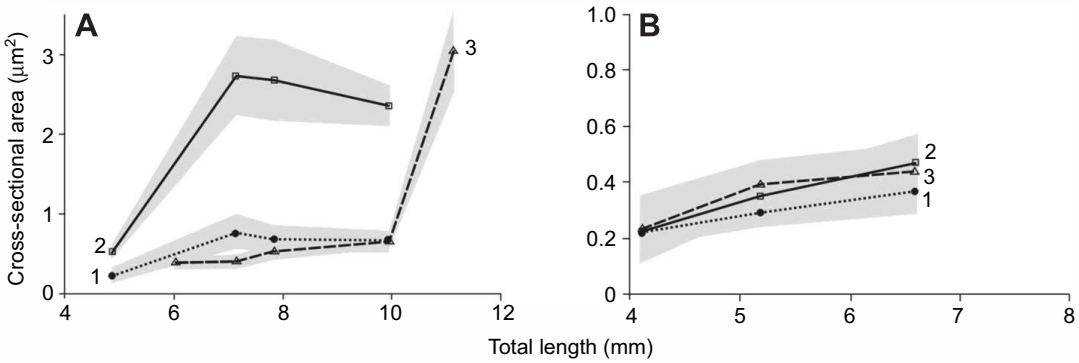

Fig. 7. Cross-sectional area (s.d. indicated by grey areas) of actinotrichia in the larval median finfold of carp (A) and zebrafish (B) against TL of the animal. Dotted line, dorsal site (1); continuous line, caudal site (2); dashed line, pre-anal site (3). In the pre-anal finfold of carp larvae under 6 mm TL, no actinotrichia were found.

exact mid-dorsal view and indisputably showing camber on one of the other projections on the same frame. Carp larvae are relatively large (TL≈5–6 mm) and show strong pigmentation, which provides good contrast for quantifying swimming scenes. Zebrafish larvae are smaller (TL≈4 mm) and create insufficient contrast to make reliable measurements. Measured angles of β (Fig. 10) varied from 176 to 160 deg. The results show a correspondence between the radius of curvature of the body and the amount of camber, i.e. more curvature (smaller r_1) leads to more camber (smaller β). It was not possible to obtain similar data for passive bending (cf. Fig. 8) using the same set-up, because the arrangement of the mirror construction inside the small aquarium did not allow fixation of the larva with one micromanipulator while its tail was bent using another, all in the focal field of the camera. The second micromanipulator then blocks the caudal view on the tail.

Model

With the help of the analytical model, we calculated the amount of camber of a 5 mm TL carp larva at body curvatures observed during free swimming and at the measured values of α and l (dashed line in Fig. 10), which closely matches the measured data (filled circles). The maximal deviation of a measured value from the model prediction is 3.7%, and the mean deviation is 1.3%.

Calculations of the lateral projection area of the finfold (A_{lat}) show its variation to be negligible (≪1%) in the observed range of β.

The amount of strain in the finfold edge was calculated for different combinations of α and r_1 (Fig. 11) for swimming zebrafish and carp larvae. During swimming movements r_1<0.10 TL does not occur. Only in fast startle responses does r_1 approach this value. In a carp larva of 5 mm TL, a value of r_1=0.10 TL results in a maximal strain (ε) in the outer edge of the finfold of just below 4%. In a zebrafish larva of 4.4 mm TL, strain in the outer edge of the finfold never exceeds 1%.

DISCUSSION

General

As shown above, it is the architecture of the median finfold that causes it to camber during lateral bending of the larval body. Obliquely oriented rows of collagen bundles at the flanks of the finfold, the actinotrichia, contribute to this deformation. The increase in second moment of area results in an increased rigidity of the finfold itself and of the caudal part of the larval body as a whole, enabling fast acceleration of the larva. The (ultra-) structural details show that actinotrichia, which are under tension, are strongly anchored at their base in the skin of the trunk, while their tapering distal ends are anchored in one another, so strengthening the outer edge. This arrangement enables transmission of force from swimming muscles, which bend the body, to the median finfold. In this way, the seemingly weak structure of the larval median finfold, which more than doubles the lateral projection area of the larval body, contributes to maximizing the mass of water that is accelerated backwards during swimming movements, thus increasing the forward acceleration of the animal. This is especially important in feeding and in escape movements.

The supposed deformation of the larval finfold during swimming is confirmed by high-speed videos (Figs 4, 10), and also occurs when the body bends into a double-bent S-shape rather than a single-bent C-shape.

Furthermore, passive bends in the larva generate camber, demonstrating that camber is a passive, structural phenomenon (Figs 8, 9).

Carp

In carp larvae, the mean α measured at the three sites is between 54 and 60 deg, remaining nearly constant at the three sites during ontogeny. The change from an increase in tensile strength at the

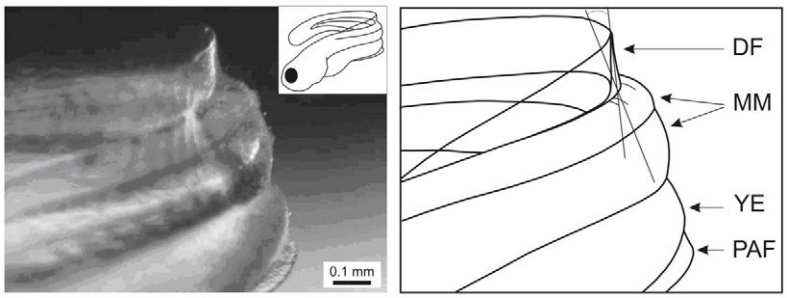

Fig. 8. Photograph (left) and schematic drawing (right) of the trunk of an anaesthetized 6 mm TL carp larva forced into a curved position (see inset for overview). DF, dorsal finfold; MM, muscle mass; YE, yolk extension; PAF, pre-anal finfold. Note the cambered dorsal and pre-anal finfold.

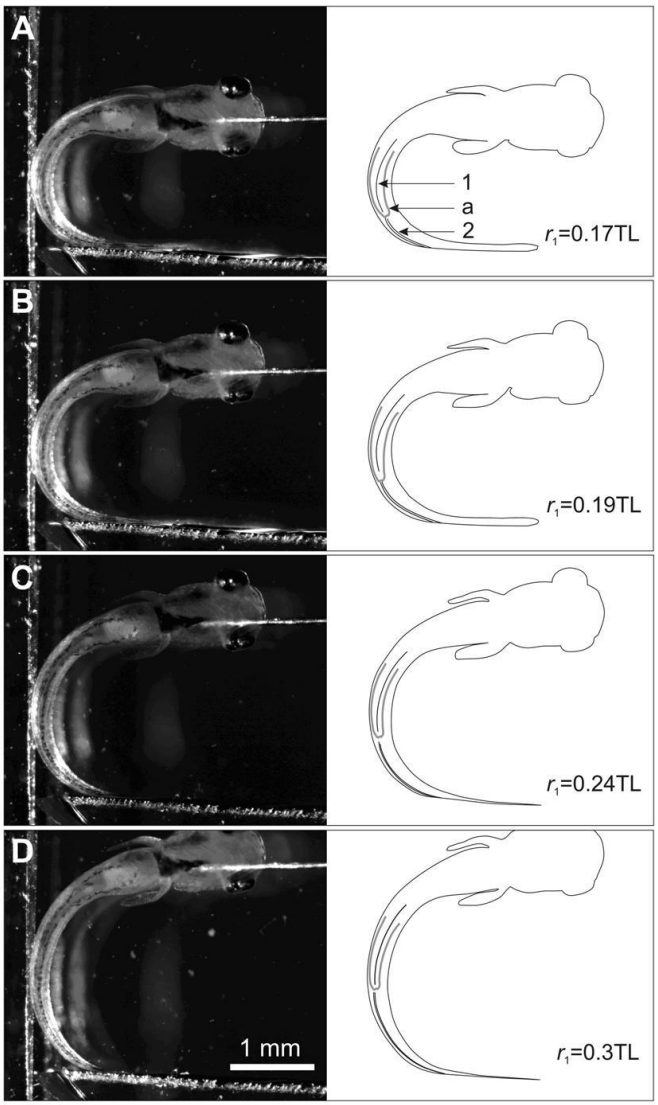

Fig. 9. Photographs (left) and schematic drawings (right) of ventral views of the pre-anal and caudal finfold of a TL=5.2 mm carp larva at different body curvatures (r_1 ranging from 0.17 TL in A to 0.3 TL in D). In all four pictures the outer edge of the pre-anal finfold (1) remains in the same vertical plane (indicated by a single line), and that of the caudal finfold (2) is cambered outwards with respect to its midbase (indicated by a double line). a, anus.

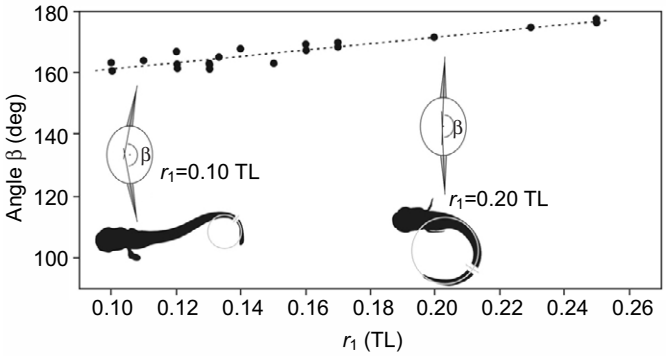

Fig. 10. Amount of camber (angle β) at the corresponding radius of curvature (r_1), measured from high-speed video images of startle responses (N=19) of carp larvae of 5 mm TL (N=5) and 6 mm TL (N=3); R^2=0.857. The stronger the body curvature (r_1 small), the higher the amount of camber (angle β small). To illustrate body curvatures of 0.10 TL and 0.20 TL, silhouettes are plotted below a schematic representation of the corresponding camber. The dashed line represents the amount of camber as predicted by the model for a 5 mm TL carp larva.

dorsal and caudal site (sites 1 and 2, Fig. 7) in carp larvae of TL<7 mm to a decrease at TL>7 mm reflects the observed change in swimming style (Osse, 1990; Osse and Van den Boogaart, 1995; Osse and Van den Boogaart, 2000) during ontogeny. Carp gradually alter their swimming style from anguilliform towards (sub)carangiform at about this size, thus reducing, relatively speaking, the magnitudes of normal and tangential reaction forces of the water along the body and increasing those in the tail. In carp larvae of TL>10 mm, no actinotrichia were found at the dorsal and caudal site. At this body size, the finfold is almost completely replaced by the true unpaired fins, and true fin rays, lepidotrichia, which probably provide rigidity and make actinotrichia superfluous.

In the pre-anal finfold (site 3), no actinotrichia were found at TL<6 mm and passive bends did not generate visible camber here (Fig. 9). In post-flexion larvae, at TL>10 mm, CSA of actinotrichia was still increasing here. This suggests a different role of this part of the median finfold. Van Snik and colleagues suggested that it might serve to obtain a favourable drag coefficient with a minimal amount of tissue and thus energy investment and/or to reduce yaw motions during swimming (Van Snik et al., 1997). Verhagen proposed an increase in propulsion efficacy of swimming fish larvae at intermediate *Re* values, by exploiting left and right alternating eddies at the tail tip, which are generated behind the undulating head (Verhagen, 2004). The larval finfold acts as a kind of splitter-plate to strengthen the two-dimensional character of the eddies as they are moving along the body towards the tail-tip. Similarly, in adult fish Tytell and colleagues remark that the efficiency of the caudal fins is boosted by the flow from the dorsal and anal fins (Tytell et al., 2008).

Zebrafish

In zebrafish larvae, the mean α measured at the three sites is roughly between 62 and 68 deg. Similar to carp, the angles remain nearly constant at the three sites during ontogeny, but overall they are larger in zebrafish than in carp. Interestingly, both carp and zebrafish have an α value of around 60 deg at site 2. In this body region of fish larvae, the highest body curvatures are found during vigorous swimming (r_1=0.10 TL) (Müller and Van Leeuwen, 2004; Osse and Van den Boogaart, 2000), resulting in maximal amounts of camber and strain, and suggesting that at this site the value of α is most critical.

The CSA, which co-determines the local tensile strength, is much lower than in carp larvae at all three sites, slightly increasing between TL=4 mm and TL=6.6 mm. Thus, the correspondence between local tensile strength at different length classes is not as strong as in carp, but one should keep in mind that flexion of the notochord tip in zebrafish occurs at a smaller body size than in carp, at TL≈6 mm, enabling (sub)carangiform swimming. So, the zebrafish data of Fig. 7 should only be compared with the left-most part of the carp data in this figure. In addition, kinematic data on swimming behaviour of zebrafish larvae (Müller and Van Leeuwen, 2004) do not show a clear transition from anguilliform to (sub)carangiform swimming, as has been reported for carp; they suggest a more gradual change of the magnitude of normal and tangential reaction forces of the water along the body of larval zebrafish swimming at different stages

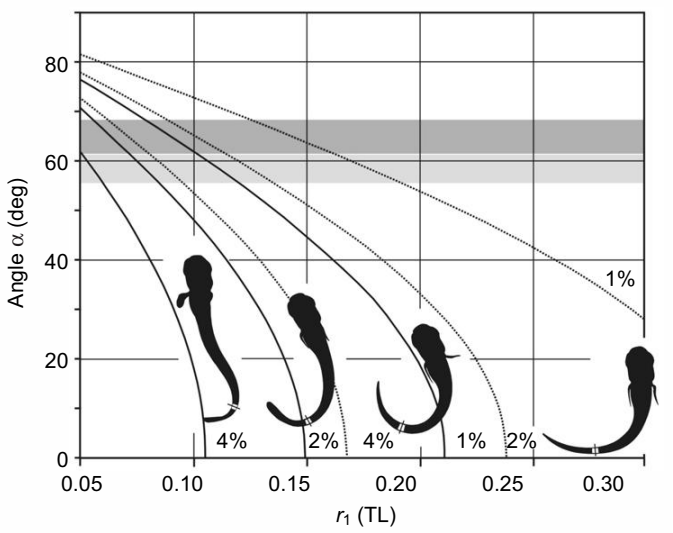

Fig. 11. Curves (calculated by the model) representing 1%, 2% and 4% strain in the edge of the finfold of a 5 mm TL carp larva (dotted lines) and a 4.4 mm TL zebrafish larva (continuous lines) as a function of α and r_1. In a carp larva of 5 mm TL, actinotrichia angle α=56 deg and actinotrichia length l=0.24 mm. In a zebrafish larva of 4.4 mm TL, α=64 deg and l=0.15 mm. To illustrate the body curvature, silhouettes derived from a high-speed movie of a startle response of a 5 mm TL carp larva are shown. The points on the tail where r_1 is 0.1 TL, 0.15 TL, 0.20 TL and 0.30 TL are marked. The horizontal grey bars represent the range of mean values of α in a carp larva of 5 mm TL (light grey, N=2), and of a zebrafish larva of 4.4 mm TL (dark grey, N=2). Strain in the edge of the finfold reaches almost 4% in carp, in extreme body curvatures during fast startle responses. Zebrafish larvae show strain of only 1% at these body curvatures.

in ontogeny. After flexion (TL≈6 mm), zebrafish change to an intermittent swimming style, with the highest body curvature in the post-anal region.

Speculating about differences

Both carp and zebrafish larvae show camber, but there is a difference in dimensions and architecture, and thus in the magnitude of camber. Considerable differences in size at maturity and in time to reach maturity (carp 20 cm, 3 years; zebrafish 3 cm, 3 months), egg diameter (1.2 and 0.7 mm, respectively) and length at hatching (4.5 and 3.2 mm TL, respectively) suggest a difference in ontogenetic scaling with respect to length, clearly visible in e.g. flexion of the notochord, which we consider as a crucial ontogenetic event in larval ecolology. In their natural habitat, zebrafish hatch and pass the flexion stage in small warm pools with aquatic vegetation where small and slow protozoans are abundant and form the preferred food, while few predators forage on the young fry (Spence et al., 2008). Laboratory cultures of zebrafish are fed with cultured *Paramecium*, only to be replaced by *Artemia* at approximately 6 mm TL.

The larger carp larvae require bigger, faster and less abundant prey items in their pre-flexion period of life. Furthermore, bigger larvae are more favourable prey for predators, making fast escape movements crucial.

So, both size at first feeding and predation would make the bigger carp larvae more dependent on their anguilliform swimming apparatus as they pass the developmental stages between hatching and flexion. This could explain the differences between the two species belonging to the same family of *Cyprinidae*.

Model

The proposed model predicts relationships between α, β, lateral propulsion area (A_{lat}) and strain (ε) in the finfold edge quite well (Figs 10, 11). At a measured value of α in a 5 mm TL carp larva the predicted β deviates on average only 1.3% from the measured β at naturally occurring body curvatures.

Strain in the edge of the finfold can be limited by properties of the longitudinally orientated tips of the actinotrichia (Fig. 2A). These tips mingle with individual collagen fibres and are interconnected with crossing (left to right) thin bundles of collagen (Fig. 6B). This arrangement results in a more or less continuous collagen band at the outer edge of the finfold, which limits the local strain to values normal for collagen, i.e. 4% (Wainwright et al., 1976). A carp larva of 5 mm TL bends its body with a radius of curvature of 10% of TL during extreme behaviours, but even then the local strain in the outer edge of the finfold, as predicted by the model, does not exceed 4% (Fig. 11). For a zebrafish larva of 4.4 mm TL, the model predicts that this strain will not exceed 1% (Fig. 11). So, a continuous collagen band in the outer edge of the finfold does not impede camber, even during extreme body curvature. The observed values of camber (Fig. 10, filled circles), inaccurate as they may be as a result of the limited quality of the video images, result in corresponding values of strain within the normal range for collagen. This result, combined with the observed typical cross-striation and the localization of collagen mRNA (Yan et al., 1995), are indications that actinotrichia are mainly composed of collagen, but further investigations of the material properties are needed (Zhang et al., 2010).

Our experimental observations prove that the finfold can withstand the normal forces of the water during oscillatory swimming movements of carp and zebrafish larvae. For a carp larva of TL=6 mm, its resistance to bending [I_y, second moment of area (see Gere and Timoshenko, 1999)] is about 2 (rostral) to 8 (caudal) times higher in a cambered position (β=160 deg) than in the vertical position (β=180 deg) based on morphology alone. So, the contribution of the increase of the second moment of area to the strength of a cambered finfold is substantial, but it is marginal compared with the resistance to bending of the larval body as a whole. Thus, fish larvae effectively increase their lateral propulsive area for effective undulating swimming.

We conclude that growth of actinotrichia in the median finfold reflects the demands imposed by changes occurring in swimming style during ontogeny. Actinotrichia form the early functional skeleton of the finfold in the absence of bony and cartilaginous structures. Camber, arising from the orientation of the actinotrichia, increases the stiffness to the finfold, resulting in more effective transmission of propulsive forces to the water. The hypothesis that the median finfold plays a role in swimming of fish larvae holds, but we cannot exclude other functions or combinations of functions [e.g. respiration (Liem, 1981)]. The universal occurrence of the relatively large median finfold in tiny fish larvae, which often only serves them for a few days, is supported by this study. However, more comparative studies are required. Our results indicate that the bio-mechanical properties of actinotrichia are similar to those of collagen, but further research is needed to determine the role of the non-collagenous proteins (Zhang et al., 2010). Feeding all data into a numerical three-dimensional finite element model will result in detailed predictions about the behaviour of the larval median finfold during swimming movements and about the flow patterns of the water. This will enable predictions of the forces generated by the larval body.

LIST OF SYMBOLS AND ABBREVIATIONS

A_{lat}	lateral projection area of the finfold
CSA	cross-sectional area
d	deviation of finfold edge from fish axis
d.p.f.	days post-fertilization
h_{trunk}	height of the trunk
l	actinotrichia length
L	considered part of finfold length
r_1	radius of curvature of larval body
r_2	radius of curvature of finfold edge
TL	total body length
α	angle between actinotrichia and longitudinal body axis
β	angle between finfolds and vertical (medial) plane
ε	strain

ACKNOWLEDGEMENTS

We thank the late G. van Snik and S. Driessen, F. Holtslag and A. Taverne-Thiele for help with collecting data. We are grateful to S. Kranenbarg, U. K. Müller, two anonymous referees and especially J. L. van Leeuwen for their extensive comments and suggestions, which improved the manuscript considerably.

FUNDING

This research received no specific grant from any funding agency in the public, commercial, or not-for-profit sectors.

REFERENCES

Batty, R. S. (1984). Development of swimming movements and musculature of larval herring (*Clupea harengus*). *J. Exp. Biol.* **110**, 217-229.

Bouvet, J. (1974). Différenciation et ultrastructure du squelette distal de la nageoire pectorale chez la truite indigène. *Archive Anatomique Microscopie* **74**, 79-96.

Dane, P. J. and Tucker, J. B. (1985). Modulation of epidermal cell shaping and extracellular matrix during caudal fin morphogenesis in the zebrafish (*Brachidanio rerio*). *J. Embryol. Exp. Morphol.* **87**, 145-161.

De Groot, J. and Van Leeuwen, J. L. (2002). Estimation of the longitudinal axis of line symmetrical soft bodies by stereophotogrammetry. *J. Biomech.* **35**, 823-827.

Doherty, P., Wasserzug, R. and Lee, J. (1998). Mechanical properties of the tadpole tail fin. *J. Exp. Biol.* **201**, 2691-2699.

Fuiman, L. A., Poling, K. R. and Higgs, D. M. (1998). Quantifying developmental progress for comparative studies of larval fishes. *Copeia* **3**, 602-611.

Fukuhara, O. (1985). Functional morphology and behaviour of early life stages of red sea bream. *Bull. Jpn. Soc. Sci. Fish.* **51**, 731-743.

Géraudie, J. (1984). Fine structural comparative peculiarities of the developing dipnoan dermal skeleton in the fins of *Neoceratodus* larvae. *Anat. Rec.* **209**, 115-123.

Géraudie, J. and Landis, W. J. (1982). The fine structure of developing pelvic fin dermal skeleton in the trout, *Salmo gairdneri*. *Am. J. Anat.* **163**, 141-156.

Gere, J. and Timoshenko, S. (1999). *Mechanics of Materials*, 4th Edn. Cheltenham, UK: Stanley Thornes Ltd.

Hunter, J. R. (1972). Swimming and feeding behaviour of larval anchovy *Engraulis mordax*. *Fish. Bull.* **70**, 821-939.

Kendall, A. W. J., Ahlstrom, E. H. and Moser, H. G. (1984). Early life history stages of fishes and their characters. Special publication no. 1 of *Ontogeny and Systematics of Fishes*, American Society for Ichtyology and Herpetology. Lawrence, KS, USA: Allen Press Inc.

Kranenbarg, S., Muller, M., Gielen, J. L. W. and Verhagen, J. H. G. (2000). Physical constraints on body size in teleost embryos. *J. Theor. Biol.* **204**, 113-133.

Liem, K. F. (1981). Larvae of air-breathing fishes as countercurrent flow devices in hypoxic environments. *Science* **211**, 1177-1179.

Liu, J., Wasserzug, R. and Kawachi, K. (1997). The three-dimensional hydrodynamics of tadpole locomotion. *J. Exp. Biol.* **200**, 2807-2819.

Müller, U. K. and Van Leeuwen, J. L. (2004). Swimming of larval zebrafish: ontogeny of body waves and implications for locomotory development. *J. Exp. Biol.* **207**, 853-868.

Nash, W. (1977). *Strength of Materials*, 2nd Edn. Schaum's Outline Series. New York: McGraw-Hill, 2nd edition.

Osse, J. W. M. (1989). A functional explanation for a sequence of developmental events in the carp. the absence of gills in early larvae. *Acta Morphologica Neerlando-Scandinavica* **27**, 111-118.

Osse, J. W. M. (1990). Form changes in fish larvae in relation to changing demands of function. *Neth. J. Zool.* **40**, 362-385.

Osse, J. W. M. and Van den Boogaart, J. G. M. (1995). Fish larvae, development, allometric growth, and the aquatic environment. *ICES J. Mar. Sci. Symposium* **201**, 21-34.

Osse, J. W. M. and Van den Boogaart, J. G. M. (2000). Body size and swimming types in carp larvae: effects of being small. *Neth. J. Zool.* **50**, 233-244.

Osse, J. W. M. and Van den Boogaart, J. G. M. (2004). Allometric growth in fish larvae, timing and function. In *The Development of Form and Function in Fishes and the Question of Larval Adaptation*, Vol. 40 (ed. J. Govoni), pp. 167-194. Bethesda, MD, USA: American Fisheries Society Syposium.

Penáz, M. (1975). Early development of the greyling *Thymallus thymallus* (Linneaus, 1758). *Acta Scientiarum Naturalium Academiae Scientiarum Bohemoslovacae Brno (Brno)* **9**, 1-35.

Rombough, P. J. (1988). Respiratory gas exchange, aerobic metabolism, and effects of hypoxia during early life. In *The Physiology of Developing Fish*, Part A, *Eggs and Larvae*, Vol. XI, *Fish Physiology* (ed. W. S. Hoar and D. J. Randall), pp. 59-161. San Diego: Academic Press, Inc.

Rombough, P. J. (2004). Gas exchange, ionoregulation, and the functional development of the teleost gill. In *The Development of Form and Function in Fishes and the Question of Larval Adaptation*, Vol. 40 (ed. J. J. Govoni), pp. 47-83. Bethesda, MD, USA: American Fisheries Society Symposium.

Ryder, J. A. (ed.) (1886). *On the Origin of Heterocercy and the Evolution of the Fins and Finrays of Fishes*. Annual report U.S. commission for fish and fisheries for 1884.

Santos-Ruiz, L., Santamaria, J. and Becerra, J. (2001). Differential expression of fgf receptors during zebrafish fin generation. *Int. J. Dev. Biol.* **45**, S131-S132.

Sire, J., Allizard, F., Babiar, O., Bourguignon, J. and Quilhac, A. (1997). Scale development in zebrafish *Danio rerio*. *J. Anat.* **190**, 545-551.

Spence, R., Gerlach, G., Lawrence, C. and Smith, C. (2008). The behaviour and ecology of the zebrafish, *Danio rerio*. *Biol. Rev.* **83**, 13-34.

Tytell, E. D., Standen, E. M. and Lauder, G. V. (2008). Escaping Flatland: three-dimensional kinematics and hydrodynamics of median fins in fishes. *J. Exp. Biol.* **211**, 187-195.

Van der Stelt, A. (1968). *Spiermechanica en myotoombouw bij vissen*. PhD thesis, University of Amsterdam (in Dutch).

Van Snik, G. M. J., Van den Boogaart, J. G. M. and Osse, J. W. M. (1997). Larval growth patterns in two ostariophysian fish (*Cyprinus carpio* and *Clarias gariepinus*) with attention to the finfold. *J. Fish Biol.* **50**, 1339-1352.

Verhagen, J. H. G. (2004). Hydrodynamics of burst swimming fish larvae; a conceptual model approach. *J. Theor. Biol.* **229**, 235-248.

Wainwright, S. A., Biggs, W. D., Currey, J. D. and Gosline, J. M. (ed.) (1976). *Mechanical Design in Organisms*. Princeton, NJ: Princeton University Press.

Wasserzug, R. (1989). Locomotion in amphibian larvae (or 'why aren't tadpoles built like fishes?'). *Am. Zool.* **29**, 65-84.

Webb, P. W. and Weihs, D. W. (1986). Functional locomotor morphology of early life history stages of fishes. *Trans. Am. Fish. Soc.* **115**, 115-127.

Weihs, D. (1980a). Energetic significance of changing in swimming modes during growth of larval anchovy, *Engraulis mordax*. *Fish. Bull.* **77**, 597-604.

Weihs, D. (1980b). Respiration and depth control as possible reasons for swimming of northern anchovy, *Engraulis mordax*, yolk-sac larvae. *Fish. Bull.* **78**, 109-117.

Westerfield, M. (1993). *The Zebrafish Book, a Guide for the Laboratory Use of Zebrafish* (*Danio rerio*). Oregon: University of Oregon Press.

Wieser, W. (1995). Energetics of fish larvae, the smallest living vertebrates. *Acta Physiol. Scand.* **154**, 279-290.

Wood, A. and Thorogood, P. (1987). An ultrastructural and morphometric analysis of an in vivo contact guidance system. *Development* **101**, 363-381.

Yan, Y.-L., Hatta, K., Riggleman, R. and Postlethwait, J. (1995). Expression of a type 2 collagen gene in the zebrafish embryonic axis. *Dev. Dyn.* **203**, 363-376.

Zhang, J., Wagh, P., Guay, D., Sanches-Pulido, L., Padhi, B. K., Korzh, V., Andrade-Navarro, M. A. and Akimenko, M.-A. (2010). Loss of fish actinotrichia proteins and the fin-to-limb transition. *Nature* **466**, 234-238.